

Scaling of singular structures in extensional flow of dilute polymer solutions

Paul Becherer^{a,*}, Alexander N. Morozov^{a,b} and
Wim van Saarloos^a

^a*Instituut-Lorentz for Theoretical Physics, Universiteit Leiden, Postbus 9506,
NL-2300 RA Leiden, The Netherlands*

^b*School of Physics, University of Edinburgh, JCMB, King's Buildings, Mayfield
Road, Edinburgh EH9 3JZ, United Kingdom*

Abstract

Recently singular solutions have been discovered in purely elongational flows of visco-elastic fluids. We surmise that these solutions are the mathematical structures underlying the so-called birefringent strands seen experimentally. In order to facilitate future experimental studies of these we derive a number of asymptotic results for the scaling of the width and extension of the near-singular structures in the FENE-P model for polymers of finite extensibility.

Key words: birefringent strands, extensional flow, stagnation point, FENE model

1 Introduction

Recently, there has been renewed interest in the properties of extensional flows of dilute polymer solutions, in particular in a class of flows known as *internal stagnation point flows*, such as the four roll mill flow and the cross-slot or cross channel flows shown in Fig. 1. Theoretical modelling of such flows has proven to be particularly challenging, and despite extensive experimental and theoretical investigation, some aspects of these flows remain to be elucidated. For example, Arratia *et al.* [1] have recently found a bifurcation to asymmetric stationary flow patterns in a cross-channel flow of a dilute polymer solution, followed by a secondary instability to time-dependent asymmetric flows. In

* Corresponding author.

Email address: becherer@lorentz.leidenuniv.nl (Paul Becherer).

spite of its simple appearance, this instability is not yet fully understood. Conversely, instabilities have been found numerically that have no clear experimental counterpart (for example, Harris and Rallison [2,3] and Xi and Graham [4]).

In traditional investigations of elongational flows, it has often been assumed, either implicitly or explicitly, that the base flow solution is the classical solution [5] of the Oldroyd-B continuum equation in which the stresses are constant in space. However, Rallison and Hinch [6] already mention singular solutions of the UCM equations that are strongly peaked at the centre line along the outflow direction, and Renardy [7] recently pointed out that these singular solutions are also relevant for $Wi < 1/2$, where they do not actually diverge, but are still singular. Although such solutions are not easy to probe numerically, recent work by Thomases and Shelley [8] shows that these solutions do emerge spontaneously in high accuracy numerical simulations of a model problem for elongational flows. One reason for this may be that, as we will discuss, the constant stress solutions typically do not satisfy the physical boundary conditions at the edges of the flow region. A natural question that therefore emerges is whether these singular solutions are the mathematical counterpart of the so-called birefringent strands that have been found experimentally [9,10,11] and numerically [12,13,14]. Such strands are thin regions of highly extended polymers along the central outgoing streamlines. A strand can modify the flow, leading to a “dip” in the observed velocity profile of the exit flow [15,16], and it seems reasonable to assume that they affect any instabilities that might occur.

The singular solutions mentioned by Renardy [7] arise in models like the UCM model which essentially assume that the polymers are infinitely extensible. A second important question that emerges from these studies is therefore how these singular solutions are modified when we consider finitely extensible polymers, as in the FENE-P model [17]. The first step in this direction was made by Renardy [7], who showed that for the Giesekus model, which limits the growth of elongational stresses, stress profiles remain smooth while stress gradients can diverge.

The aim of this article therefore is to study the scaling of the main characteristics (e.g., the width) of these singular solutions strands in a simple way, and to analyse the modifications due to the finite extensibility. Our analysis is done for the ideal case of purely elongational flow, which is a good approximation near the stagnation point. By confining the analysis to this simple case we are able to derive a number of explicit asymptotic scaling results which we hope will facilitate making the connection between the (almost) singular solutions and the birefringent strands.

Our results are consistent with results for steady flow by Renardy [7], Thomases

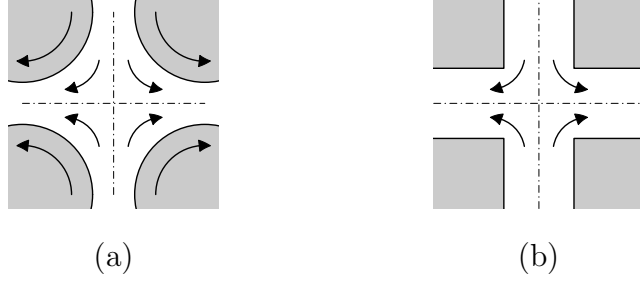


Fig. 1. (a) The four-roll mill (b) Cross-channel flow.

and Shelley [8] and Xi and Graham [4]. However, since our approach is essentially one-dimensional, we can obtain a better numerical resolution, and it may be hoped that some calculations that are not (yet) feasible in a full two-dimensional approach, such as eigenvalue calculations for stability analysis, may be performed within the framework we present here. It should be mentioned, however, that the current experimental resolution [18] is substantially worse than the numerical resolution, even for full 2-D numerics.

The layout of this paper is the following. In Section 2 we summarize the equations for extensional flow of a UCM fluid, and the structure of the singular solutions discovered recently. After analysing extensional flow of a FENE-P fluid in Section 3, we derive in Section 4 various asymptotic results for this case. We end the paper with a brief discussion of the robustness of our results.

2 Purely extensional flow of a UCM fluid

Putting the stagnation point at $(x, y) = (0, 0)$, a purely extensional flow field is given by

$$\vec{v} = (v_x, v_y) = \dot{\epsilon}(x, -y), \quad (1)$$

where $\dot{\epsilon}$ is the *elongation rate*. This flow field satisfies incompressibility, $\vec{\nabla} \cdot \vec{v} = 0$. In a nondimensionalized formulation of the UCM model, the flow field becomes

$$\vec{v} = (x, -y), \quad (2)$$

and the constitutive equation for steady flow is [5]

$$\mathbf{T} + \text{Wi} \left[(\vec{v} \cdot \vec{\nabla}) \mathbf{T} - (\vec{\nabla} \vec{v})^T \cdot \mathbf{T} - \mathbf{T} \cdot (\vec{\nabla} \vec{v}) \right] = \vec{\nabla} \vec{v} + (\vec{\nabla} \vec{v})^T. \quad (3)$$

Here \mathbf{T} is the stress tensor, \vec{v} the velocity, and Wi the *Weissenberg number*, which for purely extensional flow we define as

$$\text{Wi} = \dot{\epsilon} \lambda, \quad (4)$$

with λ the relaxation time of the polymers. The momentum conservation equation for creeping flow is

$$\vec{\nabla} \cdot \mathbf{T} - \vec{\nabla} p = 0. \quad (5)$$

Solutions for steady flow are found by inserting the pure extensional flow into the constitutive equation:

$$\begin{aligned} T_{xx} + \text{Wi} \left(x \frac{\partial T_{xx}}{\partial x} - y \frac{\partial T_{xx}}{\partial y} - 2T_{xx} \right) &= 2, \\ T_{xy} + \text{Wi} \left(x \frac{\partial T_{xy}}{\partial x} - y \frac{\partial T_{xy}}{\partial y} \right) &= 0, \\ T_{yy} + \text{Wi} \left(x \frac{\partial T_{yy}}{\partial x} - y \frac{\partial T_{yy}}{\partial y} + 2T_{yy} \right) &= -2. \end{aligned} \quad (6)$$

If we assume a spatially uniform stress field, these equations reduce to

$$T_{xx} = \frac{2}{1 - 2 \text{Wi}}; \quad T_{xy} = 0; \quad T_{yy} = \frac{-2}{1 + 2 \text{Wi}}. \quad (7)$$

It is well-known that for $\text{Wi} \geq 1/2$, this solution diverges and becomes unphysical [5]. If we no longer require that the stresses be constant in space, the stress fields lose smoothness even below $\text{Wi} = 1/2$, as was pointed out by Renardy [7]. Around and above this value of Wi , there are large stress gradients around $y = 0$, reminiscent of a birefringent strand. We shall derive these solutions, essentially following Renardy's presentation.

We choose as flow domain the strip $(x, y) \in \mathbb{R} \times [-1, 1]$. On this domain we assume pure extensional flow, see Fig. 2. We assume that the stresses depend only on y :

$$T_{xx} \equiv T_{xx}(y); \quad T_{xy} \equiv T_{xy}(y); \quad T_{yy} \equiv T_{yy}(y) = p(y), \quad (8)$$

such that momentum conservation is obeyed. We impose boundary conditions for the normal stresses on the ‘‘inflow’’ boundaries [19]:

$$T_{xx}(\pm 1) = \xi; \quad T_{yy}(\pm 1) = \eta. \quad (9)$$

The equations reduce to

$$\begin{aligned} T_{xx}(y) + \text{Wi} (-y T'_{xx}(y) - 2T_{xx}(y)) &= 2, \\ T_{xy}(y) + \text{Wi} (-y T'_{xy}(y)) &= 0, \\ T_{yy}(y) + \text{Wi} (-y T'_{yy}(y) + 2T_{yy}(y)) &= -2. \end{aligned} \quad (10)$$

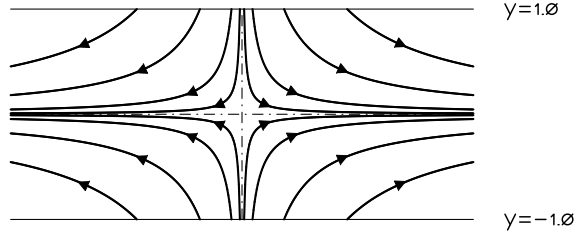


Fig. 2. Uniform extensional flow on an infinite strip.

The solution can be given in closed form¹:

$$\begin{aligned}
 T_{xx} &= \frac{2}{1 - 2 \text{Wi}} + \left(\xi - \frac{2}{1 - 2 \text{Wi}} \right) |y|^{1/\text{Wi} - 2} \\
 T_{xy} &= 0 \\
 T_{yy} &= \frac{-2}{1 + 2 \text{Wi}} + \left(\eta + \frac{2}{1 + 2 \text{Wi}} \right) |y|^{1/\text{Wi} + 2}
 \end{aligned} \tag{11}$$

The first part of the xx and yy stress components is the same as for the uniform solution (7). The second part has to be added to make the solution consistent with the imposed boundary conditions. Due to the fractional exponents in this part, none of these solutions is smooth, (except when $1/\text{Wi}$ is an integer). This becomes important when approximating these functions using spectral methods.

As Eq. (11) clearly shows, the classical constant stress solution (7) only exists for very special boundary conditions. Indeed, the non-smooth terms in Eq. (11) are present at every Weissenberg number unless one chooses $\xi = 2/(1 - 2 \text{Wi})$ and $\eta = -2/(1 + 2 \text{Wi})$. As Wi approaches $1/2$, these terms create a narrow region of large extensional stress, qualitatively similar to a birefringent strand, as was already observed by Rallison and Hinch [6].

More interestingly, the purely elongational flow, Eq. (1) does not support any boundary value for the shear stress T_{xy} other than $T_{xy} = 0$ at the boundary [19,20]. Forcing $T_{xy} \neq 0$ at the inflow would inevitably modify the velocity profile, Eq. (1): in addition to the purely extensional flow field, it would acquire a shear component. The importance of this modification will be discussed in Section 5 where we address the relevance of our results to the stability of experimental realizations of stagnation-point flows [1].

Note also that even in the range where the uniform solution clearly breaks down ($\text{Wi} \geq 0.5$), the non-uniform solution (11) is well-defined. However, the

¹ A similar solution was given in [7]. The UCM equations reported there, however, seem to be written for uniaxial extensional flow $\vec{v} = (1, -\frac{1}{2}, -\frac{1}{2})$ rather than for planar extension $\vec{v} = (1, -1)$ as claimed in [7] and as in the present paper. This explains the difference between Eq. (11) here and Eq. (9) from [7].

stress on the central outgoing streamline diverges, and for $Wi \geq 1$, the total elastic energy, which is proportional to the integral of $\text{tr } \mathbf{T}$, also diverges.

3 Extensional flow in a FENE-P model

The FENE-P model avoids the blow-up of the extensional stress by implementing a nonlinear force law for the polymer molecules [17]. The solvent is usually treated explicitly. We shall ignore the solvent viscosity, thus formulating an extension of the UCM model rather than the Oldroyd-B model.

We shall formulate the FENE-P model in terms of the *conformation tensor*

$$\mathbf{A} = \langle \vec{R}\vec{R} \rangle, \quad (12)$$

where \vec{R} is the end-to-end vector connecting two beads of a single dumbbell. The brackets denote an ensemble average.

In our nondimensionalization, the stress is given in terms of the conformation tensor as

$$\mathbf{T} = \frac{1}{Wi} \left(\frac{\mathbf{A}}{1 - \text{tr } \mathbf{A}/L^2} - \frac{\mathbf{I}}{1 - 2/L^2} \right). \quad (13)$$

Here, \mathbf{I} is the unit tensor and L^2 is the maximal value of the trace of the conformation tensor, that is, L is the maximal extension of the dumbbells, relative to their equilibrium extension. The 2 appears in the rightmost denominator because in two spatial dimensions this is $\text{tr } \mathbf{I}$.

The constitutive equation for steady flow then is [8]

$$Wi \left[(\vec{v} \cdot \vec{\nabla}) \mathbf{A} - (\vec{\nabla} \vec{v})^T \cdot \mathbf{A} - \mathbf{A} \cdot (\vec{\nabla} \vec{v}) \right] = - \left(\frac{\mathbf{A}}{1 - \text{tr } \mathbf{A}/L^2} - \frac{\mathbf{I}}{1 - 2/L^2} \right). \quad (14)$$

Note that Eqs. (13) and (14) differ from the “classical” FENE-P model in that they are restricted to two dimensions and assume the other components of the conformation tensor (A_{xz} , A_{yz} , A_{zz}) to be zero. In the two-dimensional flow Eq. (2), the classical FENE-P model [5] would have $A_{zz} \neq 0$. However, this approximation bears no influence on the asymptotic result for the width of the birefringent strand found in Section 4.

The momentum balance is nonlinear in the conformation tensor:

$$\frac{1}{Wi} \left(\frac{\vec{\nabla} \cdot \mathbf{A}}{1 - \text{tr } \mathbf{A}/L^2} + \frac{\mathbf{A} \cdot \vec{\nabla}(\text{tr } \mathbf{A})}{L^2(1 - \text{tr } \mathbf{A}/L^2)^2} \right) - \vec{\nabla} p = 0. \quad (15)$$

Again, if we assume that the conformation tensor (and, hence, the stress tensor) depends only on y , this expression simplifies, and we find one equation for A_{xx} and A_{yy} , and an equation for A_{xy} in terms of A_{xx} and A_{yy} :

$$\frac{1}{1 - \text{tr } \mathbf{A}/L^2} \left(\frac{\partial A_{yy}}{\partial y} + \frac{A_{yy}}{1 - \text{tr } \mathbf{A}/L^2} \frac{\partial \text{tr } \mathbf{A}/L^2}{\partial y} \right) - \text{Wi} \frac{\partial p}{\partial y} = 0. \quad (16)$$

and

$$\frac{1}{1 - \text{tr } \mathbf{A}/L^2} \left(\frac{\partial A_{xy}}{\partial y} + \frac{A_{xy}}{1 - \text{tr } \mathbf{A}/L^2} \frac{\partial \text{tr } \mathbf{A}/L^2}{\partial y} \right) = 0. \quad (17)$$

There are a few things to note about this system. The first equation involves only A_{xx} and A_{yy} . Suppose now that we can solve the constitutive equation (14) for A_{xx} and A_{yy} ; we can then always find a $p(y)$ to satisfy the momentum balance. From the second equation we find that *if* $A_{xy} \equiv 0$ is a solution of the constitutive equations (which in uniform extensional flow it is, as we shall see), then this always satisfies the momentum balance, similar to the UCM case. We can therefore restrict ourselves to finding a solution for the constitutive equations, given a uniform extensional flow. An analytical solution is no longer possible, and we will give numerical solutions. However, there is analytical information to be obtained from the equations, mostly asymptotics.

Analogous to the UCM case, we assume that the extension depends only on y , and we insert the pure extensional flow into the constitutive equation (14):

$$\begin{aligned} \text{Wi}(-yA'_{xx}(y) - 2A_{xx}(y)) &= - \left(\frac{A_{xx}(y)}{1 - (A_{xx}(y) + A_{yy}(y))/L^2} - \frac{1}{1 - 2/L^2} \right), \\ \text{Wi}(-yA'_{xy}(y)) &= - \frac{A_{xy}(y)}{1 - (A_{xx}(y) + A_{yy}(y))/L^2}, \\ \text{Wi}(-yA'_{yy}(y) + 2A_{yy}(y)) &= - \left(\frac{A_{yy}(y)}{1 - (A_{xx}(y) + A_{yy}(y))/L^2} - \frac{1}{1 - 2/L^2} \right). \end{aligned} \quad (18)$$

We shall use the same domain and boundary conditions as for the UCM case. For simplicity, we assume $A_{xx} = A_{yy} = 1$ (the equilibrium values) at $y = \pm 1$. It is clear that $A_{xy} \equiv 0$ is indeed a solution of the equations. We can then ignore this component of the conformation tensor, and we may restrict ourselves to the diagonal components.

For $L^2 = 10, 100, 1000$ we then find, for different Wi , the plots in Fig. 3. These are clearly qualitatively similar to the birefringent strands that have been found experimentally and numerically [9,10,11,12,13,14].

The formulation in terms of a conformation tensor allows us to translate these results immediately to a birefringence profile: for the relative change in index

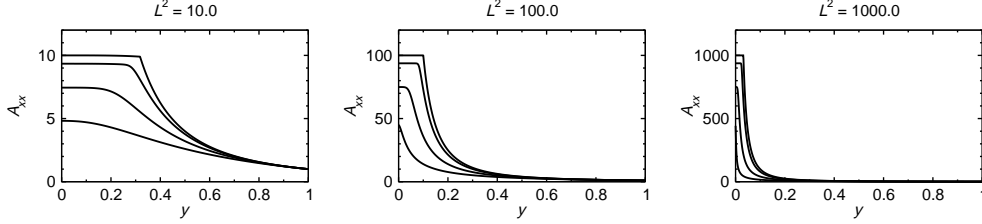


Fig. 3. Extension A_{xx} for different L^2 , for $Wi = 0.9, 2.0, 8.0$, and $Wi \rightarrow \infty$. Note the different scales on the vertical axis.

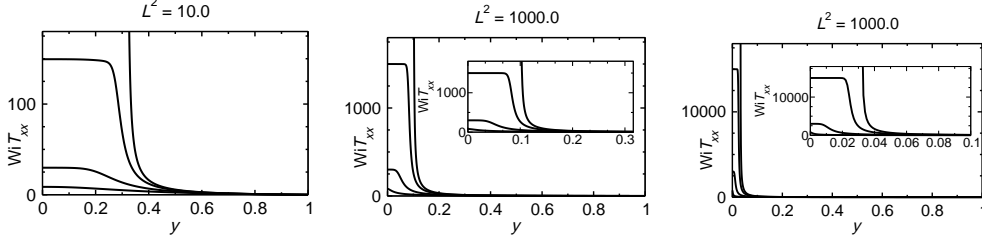


Fig. 4. Normal stress $Wi T_{xx}$ for different L^2 , for $Wi = 0.9, 2.0, 8.0$ and $Wi \rightarrow \infty$. Note the different scales on the vertical axis. The insets show a smaller range.

of refraction n , we have the proportionality [21]

$$\frac{\Delta n}{n} \propto \sqrt{(A_{yy} - A_{xx})^2 + 4A_{xy}^2}. \quad (19)$$

For the strongly stretched central region, the birefringence is approximately directly proportional to A_{xx} .

For the stresses, we can use Eq. (13). Since in our nondimensionalization, the *physical* stress is given by $\eta Wi \mathbf{T}$, with η the viscosity, we plot $Wi T_{xx}$ rather than T_{xx} in Figure 4.

4 Asymptotic results for a FENE-P fluid

We present four types of asymptotic results. The first is the behaviour of the flanks of the strand. Here we shall find that we recover the UCM behaviour. Next, we look at the maximal “extension” A_{xx}^o of the strand — the value of A_{xx} at $y = 0$. It depends on Wi and L^2 . We then combine these results, and give an approximate expression for the width of the strand, which we define as the point where the UCM profile intersects A_{xx}^o . We also show that this gives practically the same results as another definition for the width, namely the inflection point of the A_{xx} profile. Last, we look at the behaviour of the extension around $y = 0$, and we show that even though the stresses at the centre stay finite, stress *gradients* may diverge for $y \rightarrow 0$.

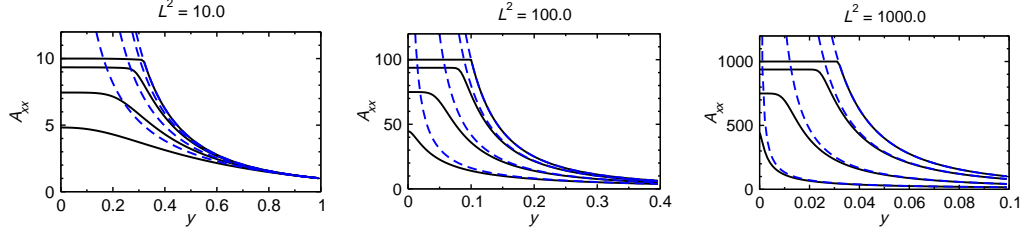


Fig. 5. Extension A_{xx} , *solid line*, compared to “UCM extension” $WiT_{xx} + 1$, *dashed line*, for different L^2 , for $Wi = 0.9, 2.0, 8.0$ and $Wi \rightarrow \infty$. Note the different scales on both axes.

4.1 Outer flanks

For small extensions, the FENE dumbbells behave approximately as linear springs. We would therefore expect to recover UCM behaviour outside the centre of the strand, where the extension is relatively low.

To compare the FENE-P profiles to the UCM results, note that from Eq. (13) we find that for small extension at large L^2

$$\mathbf{T} \approx \frac{1}{Wi}(\mathbf{A} - \mathbf{I}) \quad \text{for} \quad \text{tr} \mathbf{A} \ll L^2 \quad \text{and} \quad L^2 \gg 1. \quad (20)$$

For the xx component, this implies

$$WiT_{xx} \approx A_{xx} - 1. \quad (21)$$

For the present boundary conditions, this means that outside the centre of the strand, we have

$$A_{xx} \approx WiT_{xx}^{\text{UCM}} + 1 = \frac{2Wi}{1 - 2Wi} \left(1 - |y|^{1/Wi-2}\right) + 1. \quad (22)$$

This approximation also works well for very high Wi , because the right hand side of Eq. (14) is then negligible, until $\text{tr} \mathbf{A}$ comes very close to L^2 . Note that we compare the UCM *stress* with the FENE-P *extension*. For the small extension limit, the comparison of the *stresses* in both models also gives good results (in that case, the approximation (21) holds well), but it breaks down in the large Wi limit.

If we compare the profiles for the conformation tensor to the solution for the UCM fluid, as in Fig. 5, we see that for Weissenberg number above roughly 1.0, the flanks of the stress profile are approximated by those of the UCM case, cut off in the centre by the value of A_{xx} at $y = 0$. This observation helps us to obtain some asymptotic analytical results for the structure of the birefringent strand.

4.2 Maximal extension

We can find the maximal extension by taking the limit of the equations (14) and (15) for $y \rightarrow 0$. The advection terms then vanish, and we are left with the system

$$-2 \text{Wi} A_{xx} = - \left(\frac{A_{xx}}{1 - \text{tr} \mathbf{A}/L^2} - \frac{1}{1 - 2/L^2} \right), \quad (23a)$$

$$2 \text{Wi} A_{yy} = - \left(\frac{A_{yy}}{1 - \text{tr} \mathbf{A}/L^2} - \frac{1}{1 - 2/L^2} \right). \quad (23b)$$

This system does not allow a simple analytical solution. However, we can make a fair approximation by assuming that $A_{xx} \gg A_{yy}$ and $A_{xx} \gg 1$ (this requires $L^2 \gg 1$). We then have an autonomous equation for A_{xx} :

$$-2 \text{Wi} A_{xx} = - \left(\frac{A_{xx}}{1 - A_{xx}/L^2} \right). \quad (24)$$

This is easily solved and gives

$$A_{xx} = L^2 \left(1 - \frac{1}{2 \text{Wi}} \right). \quad (25)$$

This approximation can be shown to be self-consistent. For $\text{Wi} \gtrsim 2$, clearly $A_{xx} \gg 1$. Furthermore, since the flow is purely compressive in the y -direction, we expect $A_{yy} \leq 1$. In fact, we can find an asymptotic expression for A_{yy} at $y = 0$ from Eq. (23b). For large L^2 , the rightmost term is approximately 1, and assuming $A_{yy} \ll A_{xx}$, the equation simplifies to

$$2 \text{Wi} A_{yy} - \frac{A_{yy}}{1 + A_{xx}/L^2} = 1. \quad (26)$$

Inserting the asymptotic expression (25) for A_{xx} , we find

$$A_{yy} = \frac{1}{4 \text{Wi}}. \quad (27)$$

For large L and $\text{Wi} \gtrsim 2$, this implies that A_{yy} is of $O(1/L^2)$ compared to A_{xx} , and the above approximation is self-consistent. We conclude that for $L^2 \gg 1$ and $\text{Wi} \gtrsim 2$, Eq. (25) is a reasonable approximation.

This is confirmed by numerical solution of the system (23). In Fig. 6 we show the maximum value of A_{xx} as a function of Wi for different L^2 .

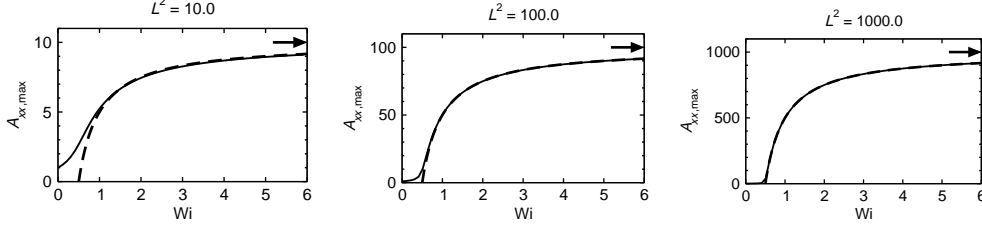


Fig. 6. Maximum of A_{xx} as a function of Wi for different L^2 . Numerical solution, *solid line*, compared with the approximation (25), *dashed line*. The arrow indicates the asymptotic value L^2 for $Wi \rightarrow \infty$. Note the different scales on the vertical axis.

4.3 Width of the birefringent strand

Given these results, we can now proceed to derive an approximation for the width of the birefringent strand as a function of Wi and L^2 . We define the width as the location where the UCM approximation intersects the value of the “centre maximum” of the extension. This is essentially the width of the “plateau” in Fig. 3.

We combine the results in eqs. (11), (21) and (25) to obtain for the intersection point y_0

$$\frac{2Wi}{1-2Wi} \left(1 - |y_0|^{1/Wi-2}\right) + 1 = L^2 \left(1 - \frac{1}{2Wi}\right). \quad (28)$$

Solving for y_0 thus gives the strand half-width as

$$y_0 = \left[\frac{1}{2Wi} + L^2 \left(1 - \frac{1}{2Wi}\right) \right]^{Wi/(1-2Wi)}. \quad (29)$$

For $Wi \rightarrow \infty$ we find $y_0 \rightarrow 1/L$. An expansion around $Wi = \infty$ gives

$$y_0 \approx \frac{1}{L} + \frac{2L^2(1 - \ln L) - 1}{4L^3} \frac{1}{Wi} + O\left(\frac{1}{Wi^2}\right). \quad (30)$$

For $L^2 \gg 1$ this reduces to

$$y_0 \approx \frac{1}{L} + \frac{1 - \ln L}{2L} \frac{1}{Wi} + O\left(\frac{1}{Wi^2}\right). \quad (31)$$

The strand half-width in these approximations is shown in Fig. 7 for different values of L^2 . Note that the “exact” solution (29) bends up for lower Wi . This is unphysical. It shows up because both sides of Eq. (28) are approximations that break down for relatively small L^2 and Wi .

The asymptotic value $1/L$ has already been found by Mackley and coworkers [10], in a more qualitative way.

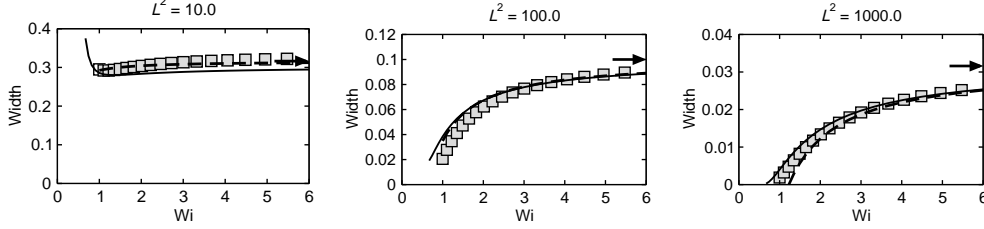


Fig. 7. Width of the birefringent strand as a function of Wi for different L^2 . “Exact” solution, Eq. (29), *solid line*, compared with the approximation (31), *dashed line*. The arrow indicates the asymptotic value $1/L$, and the *squares* denote a numerical result where the width is defined by the inflection point of the stress profile. Note the different scales on the vertical axis.

4.4 Central region

The behaviour of the extension (and, hence, the normal stresses) as $y \rightarrow 0$, is not immediately clear from the plots in Figures 3 and 4. In particular, the question arises whether the stresses display singular behaviour for $y \rightarrow 0$, as was found by Renardy for the Giesekus model [7].

It is clear from Eq. (18) that $y = 0$ is a singular point of this system of differential equations: as $y \rightarrow 0$, the highest-order derivative vanishes. The conformation tensor will therefore not be analytical in y at $y = 0$. To determine the degree of this singularity, we follow the usual procedure for dealing with singular points [22], and we expand the solution around $y = 0$ as

$$\mathbf{A}(y) = \sum_{r=0}^{\infty} \mathbf{a}_r y^{\beta+r} + \mathbf{A}_0, \quad (32)$$

with β in general non-integer, and \mathbf{A}_0 the uniform solution of Eqs. (23). We then seek an expression for the exponent β of the dominant (lowest-order) term by balancing the leading-order singular terms. For the small-extension limit, the equations actually reduce to the UCM equations, and the exponent is given by the exact solution Eq. (11), that is,

$$\beta = \frac{1}{Wi} - 2 \quad \text{for} \quad \text{tr} \mathbf{A} \ll L^2. \quad (33)$$

For moderate to high extension, we need to take into account the finite extensibility of the polymers. To lowest nontrivial order in y , the expansion (32) becomes, in components,

$$\begin{aligned} A_{xx}(y) &= A_{xx}^o + a_{xx}y^\beta, \\ A_{yy}(y) &= A_{yy}^o + a_{yy}y^\beta. \end{aligned} \quad (34)$$

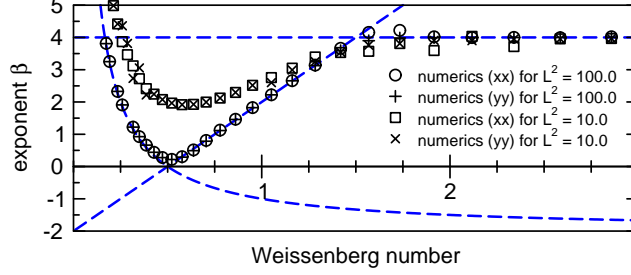


Fig. 8. The exponent β as a function of Wi . The dashed lines are the asymptotic approximations: the curve is from Eq. (33), the two straight lines are from Eq. (38). The dots were calculated from numerical solutions for a_{xx} and a_{yy} .

We insert this into the constitutive equations (14) for purely extensional flow, and expand the fractions in that equation to first order in a_{xx} and a_{yy} . We then have at first order, leaving out the constant terms (which form the equation for \mathbf{A}_0),

$$\begin{aligned} \frac{a_{xx}}{1 - \text{tr } \mathbf{A}_0/L^2} + \frac{A_{xx}^o(a_{xx} + a_{yy})/L^2}{(1 - \text{tr } \mathbf{A}_0/L^2)^2} - 2 Wi a_{xx} - \beta Wi a_{xx} &= 0, \\ \frac{a_{yy}}{1 - \text{tr } \mathbf{A}_0/L^2} + \frac{A_{yy}^o(a_{xx} + a_{yy})/L^2}{(1 - \text{tr } \mathbf{A}_0/L^2)^2} + 2 Wi a_{yy} - \beta Wi a_{yy} &= 0. \end{aligned} \quad (35)$$

We can simplify these equations considerably. We put $A_{yy}^o \rightarrow 0$, because according to (23b) it is of order $1/L^2$ compared to the other terms and also compared to $1 - A_{xx}^o/L^2$. We then substitute the asymptotic result (25) for A_{xx}^o . Since the system is linear in a_{xx} and a_{yy} , we can scale them such that

$$a_{xx} = 1 \quad \text{and} \quad a_{yy} = \gamma, \quad (36)$$

where γ is the ratio a_{yy}/a_{xx} . We are then left with the system

$$\begin{aligned} Wi[(4 Wi - 2)(1 + \gamma) - \beta] &= 0, \\ Wi \gamma(\beta - 4) &= 0, \end{aligned} \quad (37)$$

which has two solutions:

$$\gamma = 0, \quad \beta = 4 Wi - 2 \quad \text{and} \quad \gamma = -\frac{2 Wi - 3}{2 Wi - 1}, \quad \beta = 4. \quad (38)$$

The three asymptotic results for β in Eqs. (33) and (38) are plotted in Figure 8, together with numerical results for $L^2 = 10.0$ and $L^2 = 100.0$. These were obtained by integrating the differential equations (18) numerically from $y = 10^{-10}$ to $y = 1.0$ and taking the slope in a log-log representation of a_{xx} and a_{yy} . Because the stress is a regular function of the extension, these exponents immediately carry over to the stresses around $y = 0$.

From the asymptotic results, we can conclude the following: although the stresses themselves remain finite for any Weissenberg number, for sufficiently large L there is a range of Wi for which $\beta < 1$ and stress gradients become infinite. This range lies roughly between $Wi = 1/3$ and $Wi = 3/4$. These bounds are obtained by putting $\beta = 1$ in Eqs. (33) and (38). The range is finite, because for low Wi the velocity gradient is insufficient to cause large extension gradients, while for high Wi the polymers are already almost fully stretched well outside of the central region, which also prevents the formation of large extension gradients in the central region (as can be seen in Fig. 5).

The precise extent of the range in Wi for which the stress gradient diverges, depends on L^2 ; for small L^2 it is absent entirely, as can be seen in Fig. 8 for $L^2 = 10.0$. Although the analysis in the present paper is less straightforward, it is fully analogous to Renardy's result for the Giesekus model [7].

5 Concluding remarks

The results that we have derived here are valid for a rather artificial geometry, namely a purely extensional flow on an infinite strip. However, we believe that the results are still relevant for more realistic flows. The approximation that quantities do not depend on x is valid on the central incoming flow line. If we can show that the results do not depend crucially on the exact boundary conditions and on the assumption of uniform extensional flow, then the results that were derived above still give information on the shape of actual birefringent strands in fluids that are described by the FENE-P model.

We hope that our results for the scaling behaviour of these near-singular structures will stimulate new experiments on the birefringence strands — we surmise that the birefringent strands seen experimentally are indeed the experimental realizations of these structures, but the data on these in the existing literature lack the precision to test this claim.

Finally, we make a connection between our results and the recently observed instabilities in the cross-channel flow [1] (see Fig. 1b). There, the fully-developed (or being close to it) Poiseuille flow in the inlet channels provides boundary conditions for the normal and shear components of the stress tensor (T_{yy} and T_{xy} in our notation) at the inflow boundaries of the square region in the centre of the flow domain. These boundary conditions clearly differ from the special values discussed in Section 2, and thus the flow in the central region is *not* a constant-stress solution as Eq. (7) and is expected to be dominated by strands similar to (11). Moreover, the non-zero value of the shear stress and the parabolic profile of the velocity at the boundaries imply that the actual flow in the central domain is a combination of elongational and shear

components. One might then argue that the first instability observed in [1] corresponds to switching from elongation-dominated to shear-dominated velocity field, while the second bifurcation would be a purely elastic instability of that shear-dominated flow with curved streamlines [23,24]. The latter are almost always Hopf bifurcations [23,24] which is consistent with the time-dependent flows observed in [1] at large Weissenberg numbers. Our results can be considered to be a first step in constructing an analytic approximation to the base flow in the cross-channel geometry which can then be used in linear stability analysis. Inclusion of finite extensibility is likely to be important in studies of the secondary instability.

References

- [1] P. E. Arratia, C. C. Thomas, J. Diorio, J. P. Gollub, Elastic instabilities of polymer solutions in cross-channel flow, *Phys. Rev. Lett.* 96 (2006) 144502.
- [2] O. J. Harris, J. M. Rallison, Start-up of a strongly extensional flow of a dilute polymer solution, *J. Non-Newtonian Fluid Mech.* 50 (1993) 89–124.
- [3] O. J. Harris, J. M. Rallison, Instabilities of a stagnation point flow of a dilute polymer solution, *J. Non-Newtonian Fluid Mech.* 55 (1994) 59–90.
- [4] L. Xi, M. D. Graham, A mechanism for oscillatory instability in viscoelastic cross-slot flow, Submitted to *J. Fluid Mech.*, [arXiv:physics/0703262](https://arxiv.org/abs/physics/0703262) (2007).
- [5] R. B. Bird, C. F. Curtiss, R. C. Armstrong, O. Hassager, Dynamics of polymeric liquids, 2nd Edition, Vol. 1. Fluid Mechanics, Wiley, New York, 1987.
- [6] J. M. Rallison, E. J. Hinch, Do we understand the physics in the constitutive equation?, *J. Non-Newtonian Fluid Mech.* 29 (1988) 37–55.
- [7] M. Renardy, A comment on smoothness of viscoelastic stresses, *J. Non-Newtonian Fluid Mech.* 138 (2006) 204–205.
- [8] B. Thomases, M. Shelley, Emergence of singular structures in Oldroyd-B fluids, *Phys. Fluids* 19 (2007) 103103.
- [9] M. Mackley, A. Keller, Flow induced polymer-chain extension and its relation to fibrous crystallization, *Phil. Trans. Roy. Soc. London A* 278 (1975) 29–66.
- [10] D. G. Crowley, F. C. Frank, M. R. Mackley, R. G. Stephenson, Localized flow birefringence of polyethylene oxide solutions in a four roll mill, *J. Polymer Sci.* 14 (1976) 1111–1119.
- [11] G. G. Fuller, L. G. Leal, Flow birefringence of dilute polymer solutions in two-dimensional flows, *Rheol. Acta* 19 (1980) 580–600.
- [12] O. G. Harlen, E. J. Hinch, J. M. Rallison, Birefringent pipes: the steady flow of a dilute polymer solution near a stagnation point, *J. Non-Newtonian Fluid Mech.* 44 (1992) 229–265.

- [13] J. Feng, L. G. Leal, Numerical simulations of the flow of dilute polymer solutions in a four-roll mill, *J. Non-Newtonian Fluid Mech.* 72 (1997) 187–218.
- [14] J. Remmelgas, P. Singh, L. G. Leal, Computational studies of nonlinear elastic dumbbell models of Boger fluids in a cross-slot flow, *J. Non-Newtonian Fluid Mech.* 88 (1999) 31–61.
- [15] Y. Rabin, F. S. Henyey, D. B. Creamer, Flow modification by polymers in strong elongational flows, *J. Chem. Phys.* 85 (1986) 4696–4701.
- [16] O. G. Harlen, J. M. Rallison, M. D. Chilcott, High-Deborah number flows of dilute polymer solutions, *J. Non-Newtonian Fluid Mech.* 34 (1990) 319–349.
- [17] R. B. Bird, C. F. Curtiss, R. C. Armstrong, O. Hassager, Dynamics of polymeric liquids, 2nd Edition, Vol. 2. Kinetic theory, Wiley, New York, 1987.
- [18] J. A. Odell, S. P. Carrington, Extensional flow oscillatory rheometry, *J. Non-Newtonian Fluid Mech.* 137 (2006) 110–120.
- [19] M. Renardy, Inflow boundary conditions for steady flows of viscoelastic fluids with differential constitutive laws, *Rocky Mt. J. Math.* 18 (1988) 445–453.
- [20] M. A. Hulsen, J. P. P. M. v. d. Zanden, Mathematical and physical requirements for successful computations with viscoelastic fluid models, *J. Non-Newtonian Fluid Mech.* 29 (1988) 93–117.
- [21] A. Peterlin, Streaming birefringence of soft linear macromolecules, *Polymer* 2 (1961) 257–264.
- [22] C. M. Bender, S. A. Orszag, Advanced mathematical methods for scientists and engineers, McGraw-Hill, New York, 1978.
- [23] R. G. Larson, Instabilities in viscoelastic flows, *Rheol. Acta* 31 (1992) 213–263.
- [24] A. N. Morozov, W. van Saarloos, An introductory essay on subcritical instabilities and the transition to turbulence in visco-elastic parallel shear flows, *Phys. Rep.* 447 (2007) 112–143.